Nuclear Instruments and Methods in Physics Research A 599 (2009) 93–99

Contents lists available at ScienceDirect

Nuclear Instruments and Methods in Physics Research A

journal homepage: www.elsevier.com/locate/nima

Acoustic spatial localization of events in superheated droplet detectors

M. Felizardo [a,b,c,*], R.C. Martins [b], T.A. Girard [c], A.R. Ramos [a,c], J.G. Marques [a,c]

[a] Instituto Tecnológico e Nuclear, Estrada Nacional 10, 2686-953 Sacavém, Portugal
[b] Instituto de Telecomunicações, IST, Av. Rovisco Pais 1, 1049-001 Lisbon, Portugal
[c] Centro de Física Nuclear, Universidade de Lisboa, 1649-003 Lisbon, Portugal

ARTICLE INFO

Article history:
Received 25 June 2008
Received in revised form
8 October 2008
Accepted 16 October 2008
Available online 25 October 2008

Keywords:
Superheated droplet detectors
Instrumentation
Spatial localization

ABSTRACT

We present a method for the spatial localization of bubble nucleation events in superheated droplet detectors. This is accomplished in a two step procedure: event validation and localization. Validation is accomplished through the application of signal processing techniques including wavelets, Chirp-Z transforms and pulse shape identification procedures, to the acoustical event record to filter out electromagnetic noise and background events which would otherwise be included in the spatial localization step. A 2D spatial localization is demonstrated using a common passive acoustic source localization technique with a 4 element microphone array, a simple generalized cross-correlation time delay of arrival algorithm, and a hot probe at known positions inside the detector. Results yield resolutions of $\sim$1.21 mm^2 with a 90% confidence level.

1. Introduction

Acoustic source localization is of interest in many important research activities and has become a field of active study [1]. Spatial localization of an event through an array of sensors can provide additional information which serves several important purposes. Locating an event can automatically reject those that fail to satisfy prescribed criteria related to their nature or origin. The detection of phantoms, i.e., replicas of an event due to "sympathetic events" becomes easier since they can be correlated in both time and space. Another purpose, perhaps even more important, is that localization permits an event spatial density mapping, from which any biasing of direction in the events might be inferred.

A superheated droplet detector (SDD) [2] is a homogeneous suspension of superheated freon droplets ($\sim$30 μm of radius) inside a viscous elastic gel, which may undergo transitions to the gas phase upon energy deposition by incident radiation depending on whether the deposition satisfies two thermodynamically-defined threshold criteria: each droplet behaves as a micrometric bubble chamber. SDDs have been widely used in neutron dosimetry [3,4] and spectrometry [5–7]. They have been shown to comply with ICRP 60 recommendations for accuracy of measurement, real-time response, low minimum detection threshold and, most importantly, a nearly similar dose equivalent response.

Because of the SDD insensitivity to most backgrounds depositing less than $\sim$150 keV/μm, resulting from the double, thermodynamically tuneable detection thresholds, SDD application has been extended to dark matter searches [8,9]; the SIMPLE project [9] is one of two international dark matter searches using SDDs. Being rare event measurements, the sensitivity of a dark matter search is generally qualified by the amount of active mass and its exposure. In contrast to the commercially-available dosimeter SDDs with refrigerant concentrations of $\leqslant$0.1%, SIMPLE SDDs are fabricated at 1–3% [10]; at this level, the devices are generally opaque and require acoustical readout.

Despite the SDD insensitivity, there exist several sources of backgrounds to the device operation which must be discriminated. Previously, signals similar to bubble nucleation events were found to arise from pressure microleaks through the plastic SDD caps [10], dominating the detector response and reducing the SDD application sensitivity by several orders of magnitude. Improved cap construction has so far succeeded in severely reducing these events, and improved instrumentation with reduced noise levels has provided the means to discriminate them on the basis of their frequency spectrum [11].

Another background of concern is the radon contamination of the detector container glass, which diffusing into the gel may produce α-decay initiated nucleation events up to $\sim$1 mm from the interface. One way to reject these backgrounds, particularly the α-induced events, is by locating them spatially within the detector. We here report the preliminary realization of such a system. Section 2 describes the methodology behind the approach, based on the generalized cross-correlation (GCC) method for assessing time delays of arrival (TDOA) [12] between pairs of microphones within a microphone array. From the

* Corresponding author at: Instituto Tecnológico e Nuclear, Estrada Nacional 10, 2686-953 Sacavém, Portugal.
E-mail address: felizardo@itn.pt (M. Felizardo).

0168-9002/$ - see front matter © 2008 Elsevier B.V. All rights reserved.
doi:10.1016/j.nima.2008.10.018

combinatorial TDOAs of the microphone array, a maximum likelihood estimator [13] is used to determine the most probable volume element for a bubble nucleation event. Experimental measurements, including the measurement of the sound velocity in the gel medium, are presented in Section 3 and discussed in Section 4. Conclusions are drawn in Section 5.

2. Methodology

The basic approach is a hybrid of triangulation. As shown in Fig. 1, in addition to the standard single microphone (#5) mounted inside the SDD vessel, several additional microphones are positioned on the outside detector walls (#1–3) and bottom (#4).

Given a bubble nucleation event, its relative distances, d_i, from each microphone are determined by taking into account the TDOA t_i, and the velocity v, of the acoustic wave traveling through the gel:

$$d_i = v \times t_i \quad (1)$$

The signal analysis consists of a two step procedure:

- Event validation
- Spatial localization

In the initial step, for each of the data vectors, the identification of a true nucleation event is achieved through three measures. This process starts with the use of a continuous wavelet Morlet-based transform [14] as shown in Fig. 2(a), which is the wavelet transform most closely approximating the true nucleation event signal shown in Fig. 2(b); the choice is a result of a maximum likelihood study between a typical nucleation event and the several common wavelet bases, using the crest factor (ratio of the waveform peak amplitude and RMS value) as the cost function.

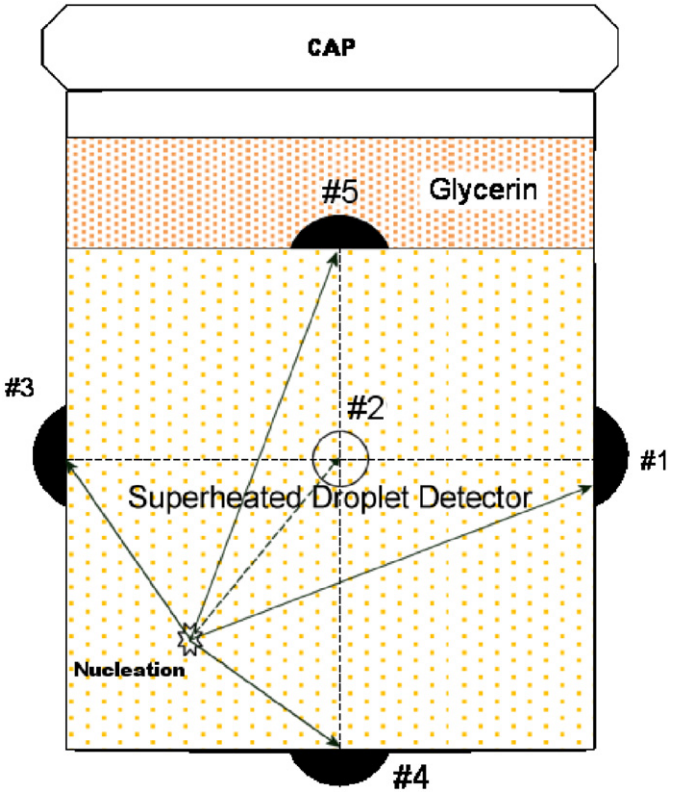

Fig. 1. Positioning of the microphones for the detector.

The crest factor provides a quick idea of what is occurring in the time waveform. The scale at which the transform is analyzed depends on the gel, the pressure, temperature and whether the microphone is inside or outside the detector. One major advantage afforded by wavelets is the ability to perform local analysis—that is, to analyze a localized area of a larger signal, and wavelet analysis is capable of revealing aspects of data that other signal analysis techniques miss, such as trends, breakdown points, discontinuities in higher derivatives, and self-similarity. In our application, it serves as a refinement for eliminating electromagnetic noise through pattern recognition.

From the output of the wavelet transform analysis, the selection of the possible candidates for nucleation events is carried out by threshold analysis, with the threshold set at 5% above noise level.

Each of the possible candidates then separately undergoes a time and frequency analysis for distinguishing true nucleation events from acoustic backgrounds. This is accomplished through a validation routine [15], which:

(i) sets an amplitude threshold;
(ii) identifies the beginning and end of each spike, based on the previous threshold;
(iii) amplitude-demodulates the time evolution of the spike;
(iv) measures the decay time constant (τ) of the pulse;
(v) suppresses the pulses which exhibit τ's below a given threshold.

The choice of the amplitude threshold is an interactive procedure, and can be set very low for the rejection of spurious noise. Amplitude demodulation is achieved simply with the modulus of the Hilbert transform of the pulse waveform, $y(t) = |H\{x(t)\}|$. After the amplitude envelope has been obtained, the maximum and the minimum of the pulse shape are determined to set the time window for evaluating τ. The decaying part of the envelope is then fit to an exponential, $h(t) = Ae^{-t/\tau}$, by means of a linear regression after linearizing the envelope, $\ln(y(t)) = \ln(A) - t/\tau + \mathrm{er}(t)$, where $\mathrm{er}(t)$ corresponds to the residual of the fit.

Fig. 3 shows a typical bubble nucleation event, and both the decay interval of the envelope and its exponential fit. An efficiency of 100% in discriminating true events from acoustic backgrounds was obtained with a τ window of 10–40 ms.

The frequency analysis is carried out for each candidate window using the Chirp-Z transform [16] and analyzing the spectrum in a 200–900 Hz window within which the oscillations of the nucleation signal are expected to be found [15]. Power spectrum (PS) analysis using fast Fourier transforms (FFTs) has been a standard SIMPLE technique for signal analyses; the Chirp-Z transform is adapted for signals with low signal-to-noise ratio, and serves to improve the frequency resolution. Fig. 4 shows the FFT from the event in Fig. 3(a). The PS is characterized by a peak at ~640 Hz, with some lower power harmonics around 2 and 4 kHz.

A final cut is applied to all surviving candidates: true nucleation signals must be present, nearly simultaneously, on all channels.

The spatial identification step, since the geometry of the problem is well known, consists of mapping the detector volume with a regular, dense, hexahedron mesh, each element with a volume of ~5 mm^3 (the voxel). For each voxel, the TDOAs of all the combinatorial pairs of the microphone array for events taking place at each voxel are computed and stored in a multidimensional matrix. The matching of the voxel with each event is carried out by a least mean square algorithm which compares the

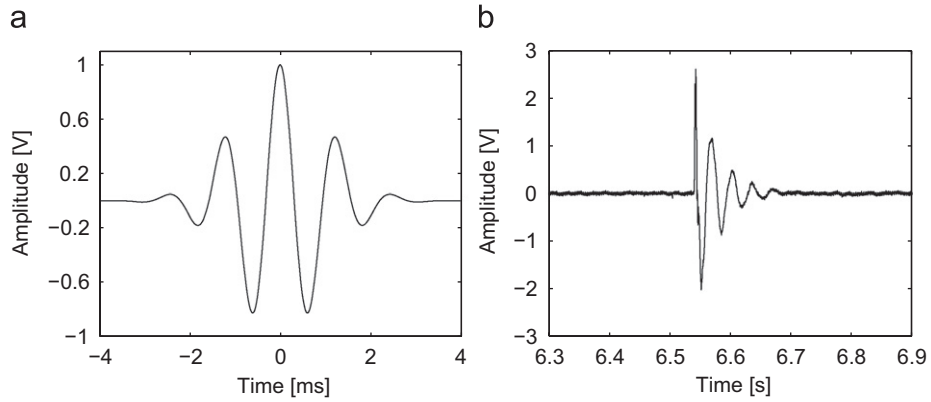

Fig. 2. (a) Morlet based transform; (b) true nucleation signal.

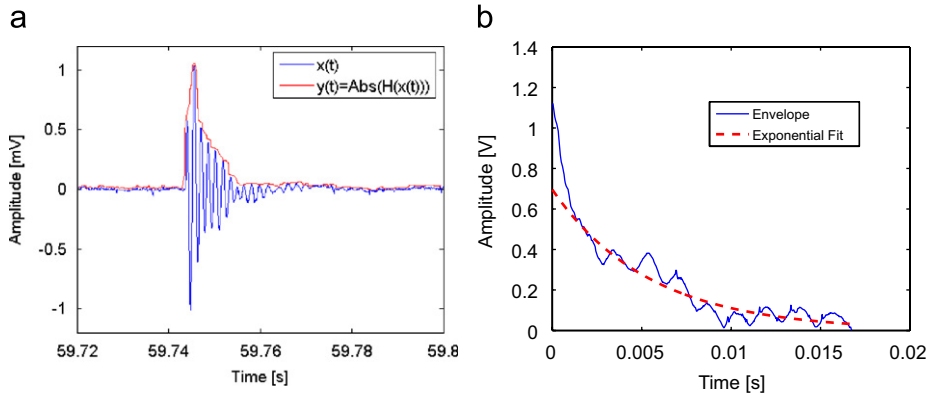

Fig. 3. Typical pulse shape (a) and (b) best fit to an exponential function of the amplitude envelope from the pulse shown in (a), with $\tau \sim 20$ ms.

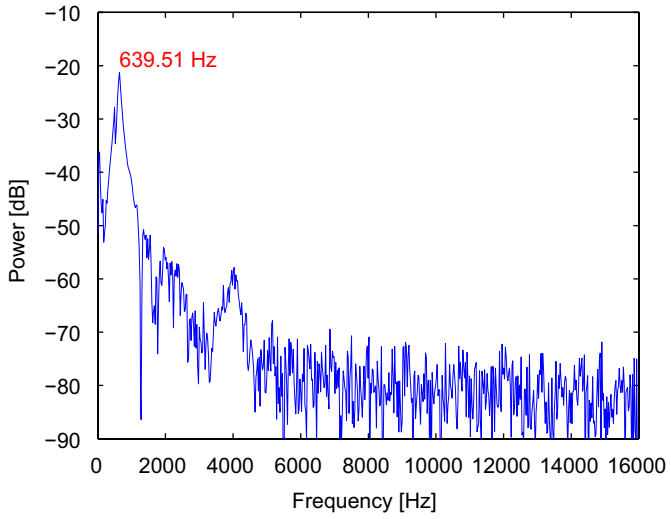

Fig. 4. Power spectrum of the bubble nucleation event.

experimental TDOAs of pairs of the microphones with the ones previously calculated and stored for each of the voxels.

The positioning of microphones outside the detector containment vessel raises the concern as to the effect of the gel–glass interface on the signal detection/analysis. While the gel–glycerin interface of the standard glycerin-immersed microphone is not an issue since the main constitution of the gel is glycerin, the gel–glass is, since one might suspect that the signals suffer a wavelength shift in transmission.

3. Experimental measurements

Three types of measurements were performed: the velocity of sound in the gel, a study of the signals recorded by the external microphones relative to the internal, and 2D spatial localization using a "hot probe" at known positions.

3.1. Measurement of the sound velocity in the gel

The velocity of sound (v) within the media needs to be accurately known as it directly relates to the spatial resolution of the system; for mm resolution, this means known to about 2–3%.

The velocity of sound in the detector gel has been previously measured as $\sim 1800\,\mathrm{ms}^{-1}$ [17]. Since the velocity varies considerably with the gel consistency and temperature, measurements were made using the standard gel of the SIMPLE detector [9].

A cylinder 2 m long with 5 cm radius was lined with acoustical shielding to prevent reflections from the walls, and filled with gel. For the acquisition, a National Instruments PXI-5105 high-speed digitizer was used, generating a short Gaussian pulse signal through the gel via a piezoelectric ceramic underwater speaker, SPS-4640-UW-01 from SONITRON. The signal was received by a waterproof microphone MR28406 from Knowles Acoustics. The measurement procedure consisted of the sound emission, with central frequency at 1 kHz and 100 Hz bandwidth, and reception; the time delay was assessed through correlation between emission (E) and reception (R), as shown in Fig. 5.

The system was calibrated in air as well as in water, at ambient conditions, with the receiver positioned at several distances (in 25 cm steps), and yielded $325.6 \pm 7.4\,\mathrm{ms}^{-1}$ and $1429.2 \pm 36.3\,\mathrm{ms}^{-1}$,

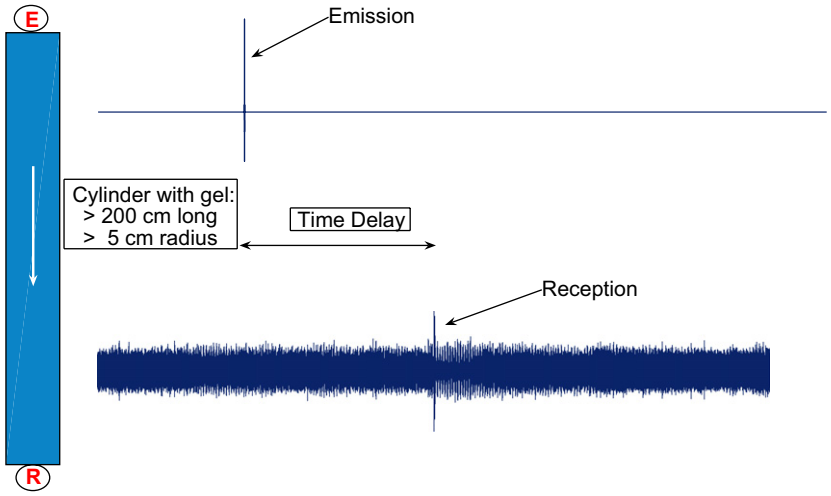

Fig. 5. Experimental set-up for the measurements of the velocity of sound in gel.

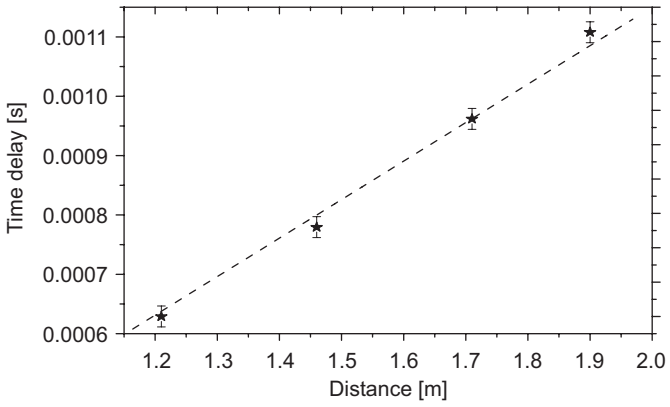

Fig. 6. Velocity of a sound wave through the gel.

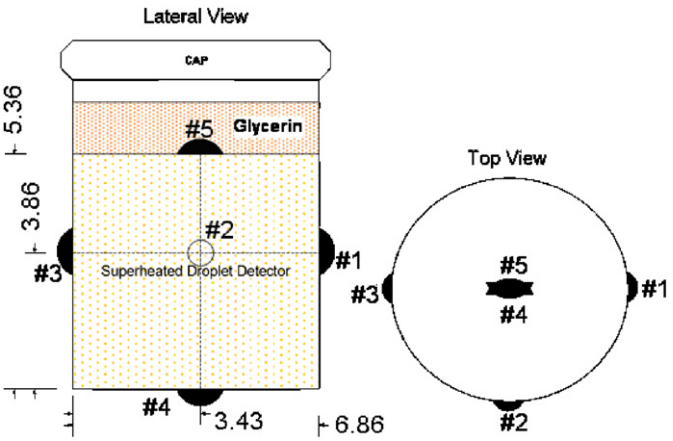

Fig. 7. Schematic of the disposition for the five microphones. Dimensions are in cm and # denotes the microphone number.

respectively. Identical measurements, with the gel installed in the tube, are shown in Fig. 6. A simple linear regression of the data gives a sound velocity in the gel of $1654.4 \pm 40.2\ \mathrm{ms}^{-1}$ at 18 °C and 72% humidity. The detector's gel is composed of glycerin (78.52%), gelatin (1.76%), bi-distilled water (16.10%) and PVP (3.62%). At operational temperatures the gel is much closer to being in a solid than a liquid state. The increase of temperature promotes the transition from solid to liquid state; therefore a decrease of sound velocity is expected and the previous measurement seems to be consistent since it was performed [17] in a water bath at 16 °C.

3.2. Gel–glass barrier

Four external microphones were glued to the outside of the vial using epoxy; a thin (1 mm) outer perimeter rubber layer was used between the microphone and the glass to avoid mechanical acoustic coupling. The fifth (standard) microphone, encased in a latex sheath, was installed inside the detector within the protective glycerin layer above the gel matrix, as in a standard detector construction. The disposition of the five microphones is shown schematically in Fig. 7.

The detector itself contained ~2.5 g of the refrigerant (CCl_2F_2) in a uniform droplet ($40 \pm 10\ \mu$m diameter) dispersion, produced according to the standard protocol for a 150 ml device [15]. It was placed in a water bath for temperature control and shielding. Measurements were made at 15 and 30 °C, well below the gel melting at 45 °C. The temperature was measured with a type k thermocouple [RS 219-4450]. Each temperature change required ~15 min stabilization time for the SDD. Data was acquired at a constant rate of 32 kSps for a period of 5 min and with a gain of 60 dB, using a Matlab platform.

These events were stimulated by environmental radiation while heating up the detector in the water bath and were cross-checked against nucleation events generated by irradiating the detectors using a quasi-monochromatic 54 keV neutron beam obtained with a Si+S passive filter at the Portuguese Research Reactor [18].

Fig. 8 shows the typical results of a measurement run. The noise level is ~7 mV for all five microphones for all temperatures. As expected, the signal amplitudes of the microphone inside the detector are higher than those attached to the sides and bottom of the detector, although at 30 °C all are the same within experimental uncertainty. At 45 °C all outside microphones recorded nucleations with amplitudes below 500 mV; the inside microphone, ~800 mV. The lines presented in the figures are the best fits to the data, without benefit of theoretical prejudice.

The time constants of the recorded events are presented in Fig. 9(a). Those of all four microphones outside the detector are

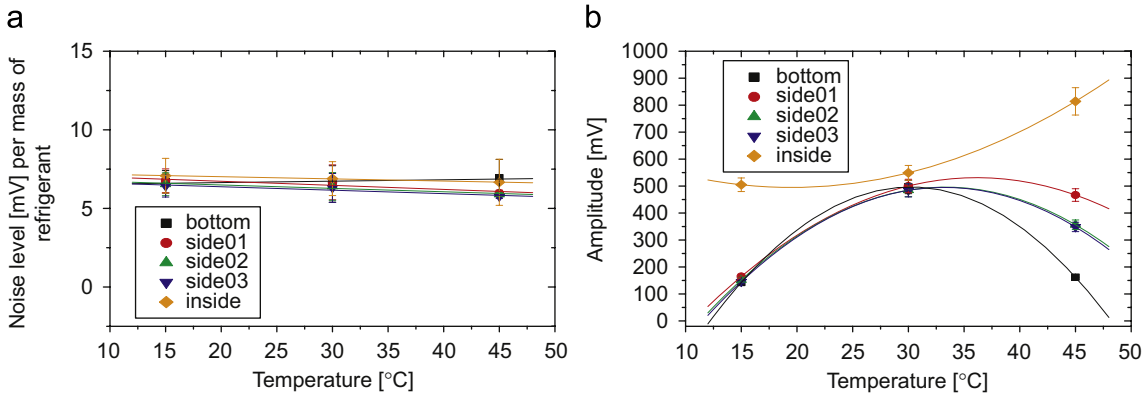

Fig. 8. Variation in (a) noise level and (b) signal amplitude for the five microphones with a standard CCl_2F_2 SDD as described in Fig. 1.

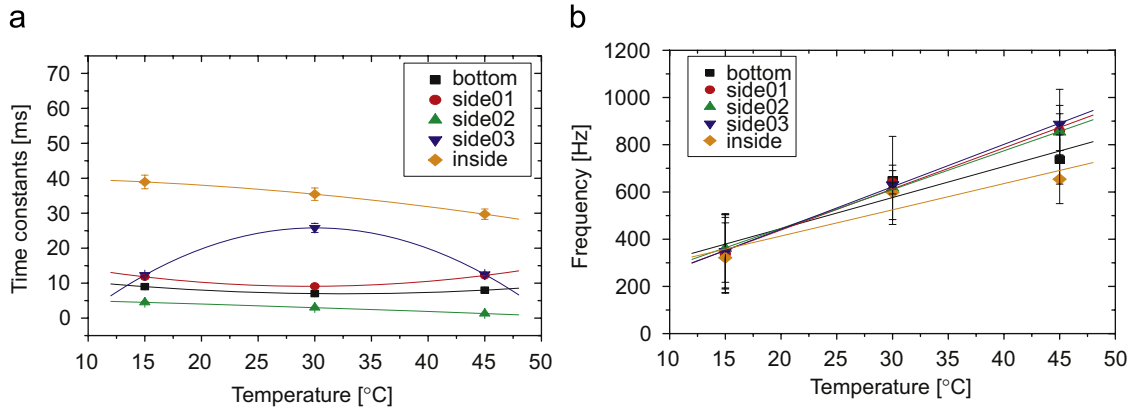

Fig. 9. Variation of signal (a) time constants and (b) frequencies for the five microphones.

low, which may be due to the wavelength shift in crossing the gel–glass interface of the detector. With the exception of microphone "side03", all τ's seem approximately constant and ~factor 4 lower than that of the microphone inside the SDD, which itself decreases slightly (40→30 ms) as the temperature of the detector rises and the gel becomes less stiff. This shift, although significant, is not critical to the validation process since the time constants remain within the 10–40 ms acceptance window for true events.

All microphones yield the same frequency for the same events within experimental errors. As shown in Fig. 9(b), only at 45 °C are the recorded frequencies of the outside microphones 10–50% higher than inside, which is most likely related to the gel's melting from the exterior towards the center due to its placement within a temperature-regulating water bath.

3.3. Spatial identification

The microphone disposition was identical to the previous tests, with the internal microphone removed to admit the entrance of a hot probe. The electronic setup was connected to the microphones using long shielded cable (~5 m). The electronic setup was itself also shielded to minimize electromagnetic noise.

The detector contained ~2.8 g of CCl_2F_2 in an uniform droplet dispersion and was produced according to the standard 150 ml device protocol [15]. It was maintained at room temperature: since a hot probe was used to stimulate nucleation events, there were no temperature variations in the experiment. The entire set-up was placed inside an acoustic foam cage constructed for the purpose of ambient noise reduction.

The hot probe consisted of a 2 mm diameter platinum rod heated by electrical resistance. The probe was inserted 1 cm deep inside the detector's gel, and roughly between microphone "side01" and "side02" (see Fig. 5). A typical transducer output is shown in Fig. 10. One can see that the three side microphones register approximately equal amplitudes for the nucleation event. The microphone placed under the detector barely recorded a signal, which is most likely due to the ~factor 2 greater probe–microphone distance than the side microphones. The difference in waveforms between the side01/side02, and side03 signals, the latter of which was about the same distance from the event, bears further study since it may contain additional information beyond the simple event occurrence.

The noise level, normalized with respect to refrigerant mass, was (5.33 ± 0.03) mV for all four microphones. The nucleation signals all have roughly the same frequency, (0.98 ± 0.16) kHz, shifted upwards from 0.6 kHz. This increase is most likely due to the increased gel temperature of the hot probe stimulation, as seen in Fig. 9(b).

The heating probe was next inserted at five angular positions at the top of the detector to depths of up to 2 cm, and heated for 20 s. Data was acquired at a constant rate of 500 kSps with a gain of 60 dB, using a Matlab platform. In this case a Keithley KUSB-3100 Series USB data acquisition hardware module was used.

The signals were processed as described in Section 2: assessing the occurrence of the events was done through the continuous Morlet waveform transform, using a new range of 0.2–1.3 kHz for

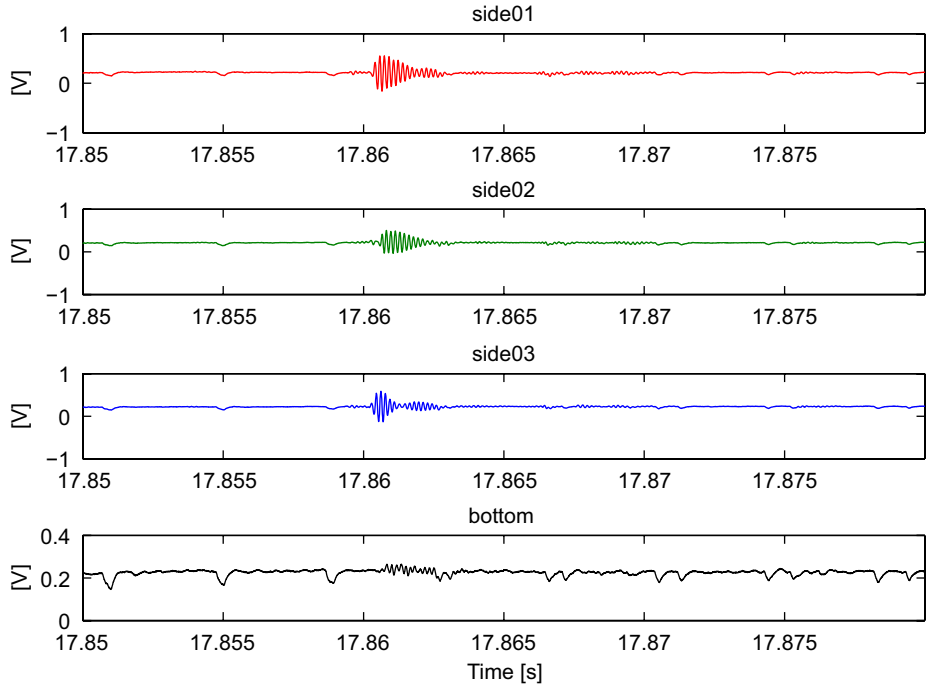

Fig. 10. Temporal evolution (pulse shape) of a typical nucleation signal, for each of the four sensors.

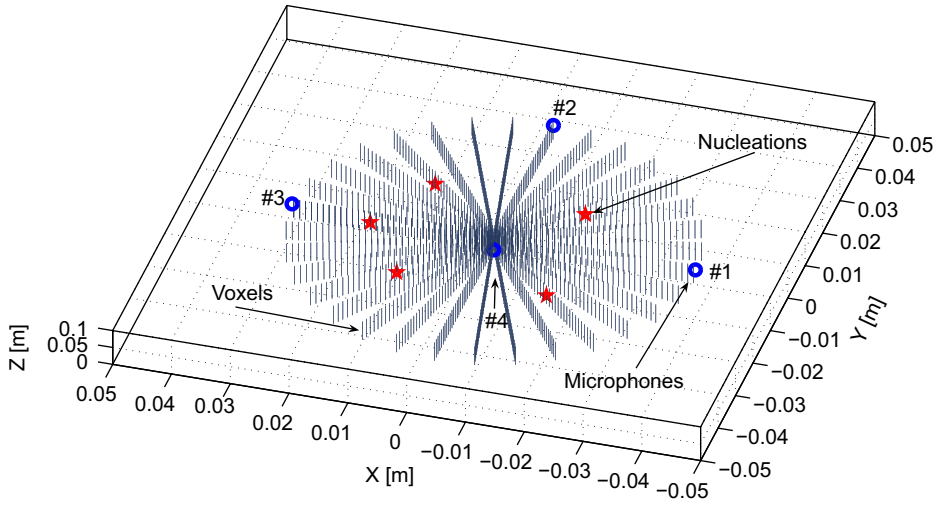

Fig. 11. Bubble nucleation map when inserting heating probes at five angular positions ($\pi/4$, $3\pi/4$, $5\pi/4$, $7\pi/4$, 0) and radius 1.71 cm at depths of 0–2 cm from the device top. The microphones identify the limits.

the Chirp-Z step, setting the time envelope for time constants between 5 and 40 ms and finally requiring a simultaneous occurrence in all channels. Once the time validation was accomplished, the spatial localization was performed by generating all delay combinations between the microphones for each of the voxels that make up the detector space. These were compared with the pre-determined delays in the multi-dimensional matrix described in Section 2, and the voxel best satisfying all delay constraints determined. Since the probe heated the emulsion along its entire length, the voxel was only truly characterized in the horizontal plane.

Fig. 11 shows a nucleation map resulting from the measurements. From these, at 1 bar pressure and room temperature (~20 °C), the resolution was 1.46 mm^2 with a 90% confidence level. The resolution was poorest along the center of the detector, especially in its middle.

4. Discussion

The determination of the time constant of a nucleation event signal and its frequency is usually enough to discriminate real from background signals. The microphones placed on the outside of the detector presented variations in the signal amplitudes, time constants and frequencies. These variations, although considerable, continue to permit discrimination through these parameters.

The spatial localization so far obtained is obviously crude in resolution, since in the forward problem we do not yet take into account the sound dispersion in the gel with a given bubble concentration, nor the reflections of the sound wave from the walls of the detector. The dependency of the gel condition on temperature also contributes to larger errors, since the velocity was used in all calculations was 1654.4 ms^{-1} determined at 18 °C. The increase of 2 °C in the gel temperature reduces the sound

Table 1
Acoustic spatial localization errors for different combinations of microphones.

Microphones				Resolution (mm^2)
Bottom (#4)	Side01	Side02	Side03	90% confidence level
x	x	x	x	1.21
x	x	x	Out	2.28
x	x	Out	x	2.02
x	Out	x	x	1.08
Out	x	x	x	1.25
Out	Out	x	x	131.80

velocity. Assuming that this decrease is linear, at 20 °C the sound velocity is $\sim$1508.8 ms^{-1}, and consequently the resolution is 1.21 mm^2 with a 90% confidence level.

The results also establish that the use of three microphones is the minimum needed to locate the voxel in a plane. As seen in Table 1, there are no major improvements when one of the microphones is not used, although the resolutions are slightly lower when the bottom (#4) and side01 microphones are not used; this is explained by the hot probe being closer to the remaining microphones.

The spatial localization tests are 2D only, since the hot probe generates a "hot line" within the gel larger than the 2 mm probe diameter, and likely produces simultaneous multiple bubble nucleations. This is likely the reason for the current resolution. A more accurate 3D testing requires development of a small diameter probe with active tip only.

5. Conclusions

We have demonstrated an approach to locate valid bubble nucleation events within the volume of a SDD. Preliminary experiments indicate a 2D localization ability with resolution a factor $\sim$2 larger than the mesh resolution (0.64 mm^2).

The experimental results are encouraging. To improve the resolution and extend the results to 3D, a new heating probe design is required. A more complete model for sound propagation within the hydrogenated gel is also required, since the velocity was measured in gel and not gel+droplet suspension, together with inclusion of glass reflections, the temperature dependence of the sound speed, and finer mesh resolution.

Acknowledgments

We thank the Portuguese Research Reactor crew at Instituto Tecnologico e Nuclear and the Department of Electrical and Computer Engineering at Instituto Superior Técnico for their contributions to these measurements. This activity was financially supported by grants, POSI/EEA-ESE/60397/2004 and POCTI/FIS/55930/2004, of the National Science Foundation of Portugal, co-financed by FEDER.

References

[1] Z. Ye, A. Alvarez, Phys. Rev. Lett. 80 (1998) 3503.
[2] R.E. Apfel, Nucl. Instr. and Meth. 162 (1979) 603.
[3] F. d'Errico, Nucl. Instr. and Meth. B 184 (2001) 229.
[4] H.W. Bonin, G.R. Desnoyers, T. Cousins, Radiat. Prot. Dosimetry 46 (2001) 265.
[5] A.R. Ramos, F. Giuliani, M. Felizardo, et al, Radiat. Prot. Dosimetry 115 (2005) 398.
[6] F. d'Errico, W.G. Alberts, G. Curzio, S. Guldbakke, H. Kluge, M. Matzke, Radiat. Prot. Dosimetry 61 (1995) 159.
[7] F. d'Errico, A. Prokofiev, A. Sanniko, H. Schuhmacher, Nucl. Instr. and Meth. A 505 (2003) 50.
[8] M. Barnabé-Heider, M. Di Marco, P. Doane, et al, Phys. Lett. B 624 (2005) 186.
[9] T.A. Girard, et al., Phys. Lett. B 621 (2005) 233.
[10] J.I. Collar, J. Puibasset, T.A. Girard, D. Limagne, H.S. Miley, G. Waysand, New J. Phys. 2 (2000) 14.1.
[11] M. Felizardo, R.C. Martins, T.A. Girard, et al., Nucl. Instr. and Meth. A 585 (2008) 61.
[12] C.H. Knapp, G.C. Carter, IEEE Trans. Acoust. Speech Signal Process. 24 (4) (1976) 320.
[13] J.C. Chen, R.E. Hudson, K. Yao, IEEE Trans. Signal Process. 50 (8) (2002).
[14] B.B. Hubbard, The World According to Wavelets: The story of a Mathematical Technique in the Making, A.K. Peters, London, 1998.
[15] M. Felizardo, R.C. Martins, A.R. Ramos, et al., Nucl. Instr. and Meth. A 589 (2008) 72.
[16] L.R. Rabiner, B. Gold, Theory and Application of Digital Signal Processing, Prentice-Hall, Englewood Cliffs, 1975, pp. 393–399.
[17] G. Waysand, private communication.
[18] F. Giuliani, C. Oliveira, J.I. Collar, et al., Nucl. Instr. and Meth. A 526 (2004) 348.